Selective cell-based smoothed finite element method using 10-node tetrahedral elements for large deformation of nearly incompressible solids

*Yuki Onishi[1]

[1]Department of Systems and Control Engineering, Tokyo Institute of Technology, Japan.
*Corresponding and Presenting author: yonishi@a.sc.e.titech.ac.jp

Abstract

A novel smoothed finite element method (S-FEM) using 10-node tetrahedral (T10) elements, SelectiveCS-FEM-T10, is proposed. In the proposed method, each T10 element is divided into T4 subelements and the strain smoothing is performed only within each T10 element, meaning no strain smoothing across elements. Also, the proposed method utilizes the selective reduced integration (SRI) technique for the stress integration. As a result, the proposed method avoids volume locking and pressure checkerboarding in nearly incompressible materials. A few examples of analysis reveal that the proposed method has good accuracy and robustness in large deformation analyses of nearly incompressible materials.

Keywords: Smoothed finite element method, Tetrahedral element, Large deformation, Volumetric locking, Pressure checkerboarding, Reaction force oscillation.

Introduction

Because of the difficulties in generating good-quality hexahedral meshes for complex shapes, finite element analyses with tetrahedral meshes are often demanded. However, it is well known that the standard tetrahedral elements are less accurate than hexahedral elements and make hard to obtain reliable results. The simplest tetrahedral element, the standard 4-node tetrahedral (T4) element, causes issues of shear locking, volume locking, and pressure checkerboarding. Although the standard 10-node tetrahedron (T10) element can resolve the issue of shear locking, it can not resolve the other issues. Moreover, it brings an additional issue of nodal reaction force oscillation. The issues of volume locking and pressure checkerboarding appear not only in rubber materials but also in materials with near incompressibility such as viscoelastic and elastoplastic materials. It is known that these issues can not be resolved at all by using finer meshes. From such a background, researches on accurate tetrahedral elements to analyze nearly incompressible materials are still being carried out actively.

The most widely used formulation as a highly accurate tetrahedral element is the mixed (hybrid) element [1, 2] based on the mixed variational principle. Various hybrid T4 or T10 elements have been proposed, but none of them has resolved all the issues above together yet. In addition, since hybrid elements require additional unknowns such as pressure, they all give rise to incompatibility with the dynamic explicit method.

On the other hand, the smoothed finite element methods (S-FEM) [3, 4] has recently attracted attention as the highly accurate tetrahedral formulations based on the pure displacement method without no additional unknowns. S-FEM is a type of strain smoothing method, and there are several formulations varied with the domains for strain smoothing: NS-FEM at nodes, ES-FEM at element edges, CS-FEM at elements and so on. We have proposed SelectiveES/NS-FEM-T4 [5, 6] combining ES-FEM-T4 and NS-FEM-T4 with the selective reduced integration (SRI) method and also F-barES-FEM-T4 [7, 8, 9, 10] combining them with the F-bar method [11]. In particular, F-barES-FEM-T4 has been proved to be a formulation that can resolve all the issues above in static analysis. However, since our previous methods require strain smoothing across elements, it is difficult to implement them as user-defined elements of general-purpose FEM codes, which is a critical problem in practical engineering.

In this research, we propose a new S-FEM formulation with T10 elements, SelectiveCS-FEM-T10, which does not perform strain smoothing across elements. Following the method of Ostien et al. [12], a dummy node is introduced at the center of each T10 element, and the element is divided into twelve T4 subelements. By performing strain smoothing only across the subelements within each element, it is possible to implement the proposed S-FEM formulation as a user-defined T10 element of general-purpose FEM codes. In addition, SRI is applied in stress integration to combine the deviatoric and hydrostatic stresses derived from two different ways of strain smoothing. As a result, the proposed method avoids all the issues above in the analyses with nearly incompressible materials. In this paper, the outline of the formulation of the proposed method is described in Section 2, and then some results of example analyses are presented to confirm the effectiveness of the proposed method in Section 3, followed by the conclusion in Section 4.

Methods

The method proposed in this paper (SelectiveCS-FEM-T10) is a type of cell-based smoothing finite element method (CS-FEM). One dummy node and twelve T4 subelements are introduced in each T10 element and the strain smoothing is performed across the subelements within each element. In contrast to the node-based S-FEM (NS-FEM), edge-based S-FEM (ES-FEM) or face-based S-FEM (FS-FEM), there is no strain smoothing across elements. The deviatoric stress is evaluated at each subelement using the smoothed strain. On the other hand, we regard the set of 12 subelements as a patch to calculate pressure in element, which is similar to the concept of F-bar Patch method [13, 14]. The final nodal force is calculated by combining them in the manner of the selective reduced integration (SRI).

Addition of a dummy node

A schematic diagram of a T10 element defined by SelectiveCS-FEM-T10 is shown in Fig. 1. The exterior 10 nodes (4 corner nodes and 6 intermediate nodes) are the same as the standard T10 element, but SelectiveCS-FEM-T10 has one additional dummy node at the element center. The position of the dummy node $\boldsymbol{x}_{10}$ is defined by the following equation as the average position of all intermediate nodes.

$$\boldsymbol{x}_{10} = \frac{1}{6}\sum_{P=4}^{9} \boldsymbol{x}_P, \tag{1}$$

where $\boldsymbol{x}_P$ represents the position vector of the node P. Since the position of the dummy node is a dependent variable, the number of unknowns does not increase. The total degrees of freedom of each element is 30: 10 nodes $\times$ 3 dimensions. Note that the edges may be bent at the intermediate nodes although the edges in Fig. 1 are all straight for simplicity.

Table 1: List of the node numbers composing each subelement. Each number denotes an intra-element subelement/node number.

Subelement Number	Node Number
0	0, 4, 6, 7
1	1, 5, 4, 8
2	2, 6, 5, 9
3	3, 7, 9, 8
4	4, 6, 7, 10
5	5, 4, 8, 10
6	6, 5, 9, 10
7	7, 9, 8, 10
8	6, 4, 5, 10
9	7, 8, 4, 10
10	8, 9, 5, 10
11	9, 7, 6, 10

Subdivision of element into subelements

An elements are subdivided into 12 T4 subelements using the 11 nodes including the dummy one as shown in Fig. 1. Table 1 shows the list of intra-element node numbers composing each subelement. Subelement 0 to 3 are located at the four corners of the element whereas Subelement 4 to 11 are located in the remaining octahedron. There are 6 edges on each subelement, and there are 30 edges in an element without duplication.

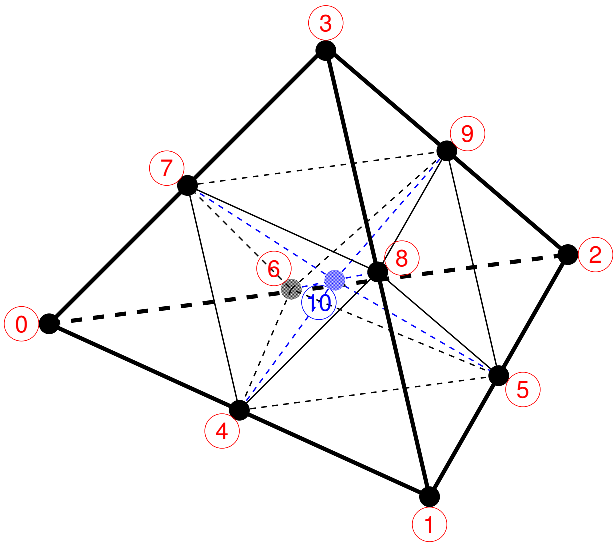

Figure 1: Schematic diagram of an element of SelectiveCS-FEM-T10. The numbers 0 to 10 denote the intra-element node numbers. Node 10 is a dummy node and is located at the average position of Node 4 to 9. An element is subdivided into 12 T4 subelements. There are 30 edges of the subelements in the element without duplication.

Shape functions of subelements and its derivatives

SelectiveCS-FEM-T10 is a T10 element but is formulated as a set of linear elements, not a quadratic elements. We consider each subelement as a standard T4 element and calculate a shape function ${}^{\mathrm{Sube}}\boldsymbol{N}$ represented by volume coordinates for each subelement. In case of the subelement using the dummy node, the weight of the dummy node is distributed to the 6 intermediate nodes evenly. As a result, the term of the dummy node can be eliminated from the shape functions. The spatial derivative of the shape function in the initial state for each subelement ${}^{\mathrm{Sube}}\boldsymbol{N}'^{\mathrm{ini}}$ ($= \mathrm{d}{}^{\mathrm{Sube}}\boldsymbol{N}^{\mathrm{ini}}/\mathrm{d}\boldsymbol{x}$) is calculated in the same fashion as the standard T4 element. Since each subelement is considered as a standard T4 element, ${}^{\mathrm{Sube}}\boldsymbol{N}'^{\mathrm{ini}}$ is constant in each subelement,

Now that ${}^{\mathrm{Sube}}\boldsymbol{N}'^{\mathrm{ini}}$ is fundamentally derived from the standard T4 element, and thus locking and pressure checkerboarding occur when we use ${}^{\mathrm{Sube}}\boldsymbol{N}'^{\mathrm{ini}}$ directly for strain evaluation. Therefore, SelectiveCS-FEM-T10 smoothes ${}^{\mathrm{Sube}}\boldsymbol{N}'^{\mathrm{ini}}$s inside the element before strain evaluation.

Smoothed derivatives of shape functions

As SelectiveCS-FEM-T10 adopts SRI, we use two kinds of smoothed spatial derivatives of shape functions for deviatoric and hydrostatic stress components. The derivative of the shape function for the deviatoric stress component is defined on each subelement (12 in total), whereas that for the hydrostatic stress component is defined only on the element. As a result, the spatial order of the hydrostatic stress is reduced in comparison to the deviatoric stress. The following shows the derivation of the derivatives.

For the deviatoric stress, we perform a cycle of smoothing. First, in the same fashion as ES-FEM-T4, the smoothed derivative on each edge (${}^{\mathrm{Edge}}\widetilde{\boldsymbol{N}'}^{\mathrm{ini}}$) is derived from ${}^{\mathrm{Sube}}\boldsymbol{N}'^{\mathrm{ini}}$s as

$$ {}^{\mathrm{Edge}}_{\quad h}\widetilde{N'}^{\mathrm{ini}}_{P,j} = \frac{1}{{}^{\mathrm{Edge}}_{\quad h}V^{\mathrm{ini}}} \sum_{k \in {}^{\mathrm{Edge}}_{\quad h}\mathbb{K}} {}^{\mathrm{Sube}}_{\quad k}N'^{\mathrm{ini}}_{P,j} \; {}^{\mathrm{Sube}}_{\quad k}V^{\mathrm{ini}}/6, \tag{2} $$

where $N'_{P,j}$ is the derivative of the shape function on Node P in the jth direction ($= \partial N_P/\partial x_j$), ${}^{\mathrm{Edge}}_{\quad h}\mathbb{K}$ denotes the set of subelements adjacent to Edge h, ${}^{\mathrm{Sube}}_{\quad k}V^{\mathrm{ini}}$ is the initial volume of Subelement k, and ${}^{\mathrm{Edge}}_{\quad h}V^{\mathrm{ini}}$ is the initial corresponding volume of Edge h ($= \sum_{k \in {}^{\mathrm{Edge}}_{\quad h}\mathbb{K}} {}^{\mathrm{Sube}}_{\quad k}V^{\mathrm{ini}}/6$). Next, using the obtained ${}^{\mathrm{Edge}}\widetilde{\boldsymbol{N}'}^{\mathrm{ini}}$s, the smoothed derivative in each subelement (${}^{\mathrm{Sube}}\widetilde{\boldsymbol{N}'}^{\mathrm{ini}}$) is derived as

$$ {}^{\mathrm{Sube}}_{\quad k}\widetilde{N'}^{\mathrm{ini}}_{P,j} = \sum_{h \in {}^{\mathrm{Sube}}_{\quad k}\mathbb{H}} {}^{\mathrm{Edge}}_{\quad h}\widetilde{N'}^{\mathrm{ini}}_{P,j}/6, \tag{3} $$

where ${}^{\mathrm{Sube}}_{\quad k}\mathbb{H}$ denotes the set of edges adjacent to Subelement k.

For the hydrostatic stress, we perform a smoothing over all subelements. The smoothed derivative on the element (${}^{\mathrm{Elem}}\widetilde{N'}^{\mathrm{ini}}_{P,j}$) is derived from ${}^{\mathrm{Sube}}\boldsymbol{N}'^{\mathrm{ini}}$s as the weighted average of all the subelements:

$$ {}^{\mathrm{Elem}}\widetilde{N'}^{\mathrm{ini}}_{P,j} = \frac{1}{{}^{\mathrm{Elem}}V^{\mathrm{ini}}} \sum_{k=0}^{11} {}^{\mathrm{Sube}}_{\quad k}N'^{\mathrm{ini}}_{P,j} \; {}^{\mathrm{Sube}}_{\quad k}V^{\mathrm{ini}}, \tag{4} $$

where ${}^{\mathrm{Elem}}V^{\mathrm{ini}}$ is the total volume of the element ($= \sum_{k=0}^{11} {}^{\mathrm{Sube}}_{\quad k}V^{\mathrm{ini}}$).

Calculation of nodal internal force

Using the two kinds of smoothed derivatives of shape functions, contributions to the nodal internal force is calculated by dividing it into two parts.

For the contribution of deviatoric stress, the deformation gradient of each subelement in the trial state (${}^{\mathrm{Sube}}\boldsymbol{F}^{+}$) is calculated as

$${}^{\mathrm{Sube}}_{k}F^{+}_{ij} = {}^{\mathrm{Sube}}_{k}\widetilde{N}'^{\mathrm{ini}}_{P,j}\, x^{+}_{P:i}, \tag{5}$$

where $\square^{+}$ denotes a trial state and $x_{P:i}$ is the jth coordinate of Node P. Putting ${}^{\mathrm{Sube}}\boldsymbol{F}^{+}$ (and its history) into the material constitutive equation, the Cauchy stress of each subelement in the trial state (${}^{\mathrm{Sube}}\boldsymbol{T}^{+}$) is obtained. The deviatoric component of ${}^{\mathrm{Sube}}\boldsymbol{T}^{+}$ is then given by

$${}^{\mathrm{Sube}}_{k}T^{(\mathrm{dev})+}_{ij} = {}^{\mathrm{Sube}}_{k}T^{+}_{ij} - \delta_{ij}\,\mathrm{trace}({}^{\mathrm{Sube}}_{k}\boldsymbol{T}^{+})/3, \tag{6}$$

where δ represents the Kronecker's delta. The contribution of the deviatoric stress to the nodal internal force $\{{}^{\mathrm{Sube}}f^{\mathrm{int(dev)}+}\}$ is calculated with the following equation.

$${}^{\mathrm{Sube}}_{k}f^{\mathrm{int(dev)}+}_{P:p} = {}^{\mathrm{Sube}}_{k}\widetilde{N}'^{\mathrm{ini}}_{P,j}\; {}^{\mathrm{Sube}}_{k}F^{+-1}_{jl}\; {}^{\mathrm{Sube}}_{k}T^{(\mathrm{dev})+}_{lp}\; {}^{\mathrm{Sube}}_{k}V^{+}, \tag{7}$$

where $f^{\mathrm{int}}_{P:p}$ represents the internal force of Node P in the pth direction.

For the contribution of hydrostatic stress, the deformation gradient of the element in the trial state (${}^{\mathrm{Elem}}\boldsymbol{F}^{+}$) is calculated as

$${}^{\mathrm{Elem}}F^{+}_{ij} = {}^{\mathrm{Elem}}\widetilde{N}'^{\mathrm{ini}}_{P,j}\, x^{+}_{P:i}, \tag{8}$$

Putting ${}^{\mathrm{Elem}}F^{+}_{ij}$ (and its history) into the material constitutive equation, the Cauchy stress of the element in the trial state (${}^{\mathrm{Elem}}\boldsymbol{T}^{+}$) is obtained. The hydrostatic component of ${}^{\mathrm{Elem}}\boldsymbol{T}^{+}$ is then given by

$${}^{\mathrm{Elem}}T^{(\mathrm{hyd})+}_{ij} = \delta_{ij}\,\mathrm{trace}({}^{\mathrm{Elem}}\boldsymbol{T}^{+})/3. \tag{9}$$

The contribution of the hydrostatic stress to $\{{}^{\mathrm{Sube}}f^{\mathrm{int(dev)}+}\}$ is calculated by the following equation.

$${}^{\mathrm{Elem}}f^{\mathrm{int(hyd)}+}_{P:p} = {}^{\mathrm{Elem}}\widetilde{N}'^{\mathrm{ini}}_{P,j}\; {}^{\mathrm{Elem}}F^{+-1}_{jl}\; {}^{\mathrm{Elem}}T^{(\mathrm{hyd})+}_{lp}\; {}^{\mathrm{Elem}}V^{+}. \tag{10}$$

Finally, the total contribution of the element to the nodal internal force is calculated as the sum of Eq. (7) and (10):

$${}^{\mathrm{Elem}}f^{\mathrm{int}+}_{P:p} = \sum_{k=0}^{11}\left({}^{\mathrm{Sube}}_{k}f^{\mathrm{int(dev)}+}_{P:p}\right) + {}^{\mathrm{Elem}}f^{\mathrm{int(hyd)}+}_{P:p}. \tag{11}$$

Calculation of tangent stiffness matrix

The tangent stiffness is obtained by calculating $\partial\{f^{\mathrm{int}}\}/\partial\{x\}$ according to the definition. Details are omitted due to the limitation of space.

Characteristics in formulation

The characteristics seen in the formulation of SelectiveCS-FEM-T10 are summarized as follows.

- It is a pure displacement-based finite element method.
  $\Longrightarrow$ It is applicable to dynamic explicit analysis unlike hybrid elements.
- There is no need to smooth strains across elements.
  $\Longrightarrow$ It can be implemented into general-purpose FEM software as a user-defined T10 element.
- The shape functions are all linear (1st-order).
  $\Longrightarrow$ It has superior robustness in large deformation; meanwhile, its mesh convergence is slower than 2nd-order elements in small deformation.
- Selective reduction integration (SRI) is used.
  $\Longrightarrow$ It is difficult to deal with material constitutive models considering pressure dependence etc.

According to our numerical experiments, the proposed one cycle strain smoothing for deviatoric stress is the optimal procedure to achieve accuracy and stability. When we perform only the edge-based smoothing within the element for deviatoric stress, no smoothing is applied to the edges of the element outline and thus shear locking occurs. On the contrary, when we repeat the cycle of strain smoothing more than once, too much smoothing is conducted and thus zero-energy mode occurs.

Results

Bending of cantilever

A large deflection cantilever bending analysis of a nearly incompressible material is performed. The analysis domain is a cuboid of $10 \times 1 \times 1$ m, its left end face is perfectly constrained, and a concentrated load in the vertical downward direction is given to the tip corner point. The material is a neo-Hookean hyperelastic body with 6 GPa initial Young's modulus and 0.499 initial Poisson's ratio. An unstructured T10 mesh with 0.2 m mesh seed size is used. In addition to the analysis with SelectiveCS-FEM-T10, analyses with ABAQUS T10 elements (C3D10, C3D10M, C3D10H, C3D10MH, and C3D10HS) are also performed using the same mesh to compare their accuracy and stability.

The distribution of Mises stress and pressure when the concentrated load is 2×10^7 N is shown in Fig. 2. The deformations are almost the same in all methods, which confirms that SelectiveCS-FEM-T10 avoids volume locking. Only ABAQUS C3D10 suffers from moderate pressure checker-boarding and the other methods including SelectiveCS-FEM-T10 are free from pressure checker-boarding. The amount of deformation at the loaded node is somewhat larger in SelectiveCS-FEM-T10 in comparison with the ABAQUS T10 elements. This might be because SelectiveCS-FEM-T10 does not use 2nd-order shape functions unlike the ABAQUS T10 and behaves more softly in large deformation. Note that the superiority or inferiority of these deformation results is difficult to be determined because of stress singularity.

Barreling of cylinder

A large deformation cylinder barreling analysis of a nearly incompressible material is performed. The analysis domain is a 1/8 of a cylinder of 1 m radius and 2 m height, symmetric boundary conditions are applied to the symmetric surfaces, and an enforced displacement to the vertical downward direction is applied to the top surface with constrains of in-plane displacements. The material is a neo-Hookean hyperelastic body with 6 GPa initial Young's modulus and 0.49 initial Poisson's ratio. An unstructured T10 mesh with 0.05 m mesh seed size is used. As in the previous example, analyses with SelectiveCS-FEM-T10 and five ABAQUS C3D10 elements are performed using the same mesh.

The distributions of Mises stress and pressure at 0.24 m enforced displacement (24% compression) are shown in Fig. 3. Although the stress distributions near the rim of the top surface are

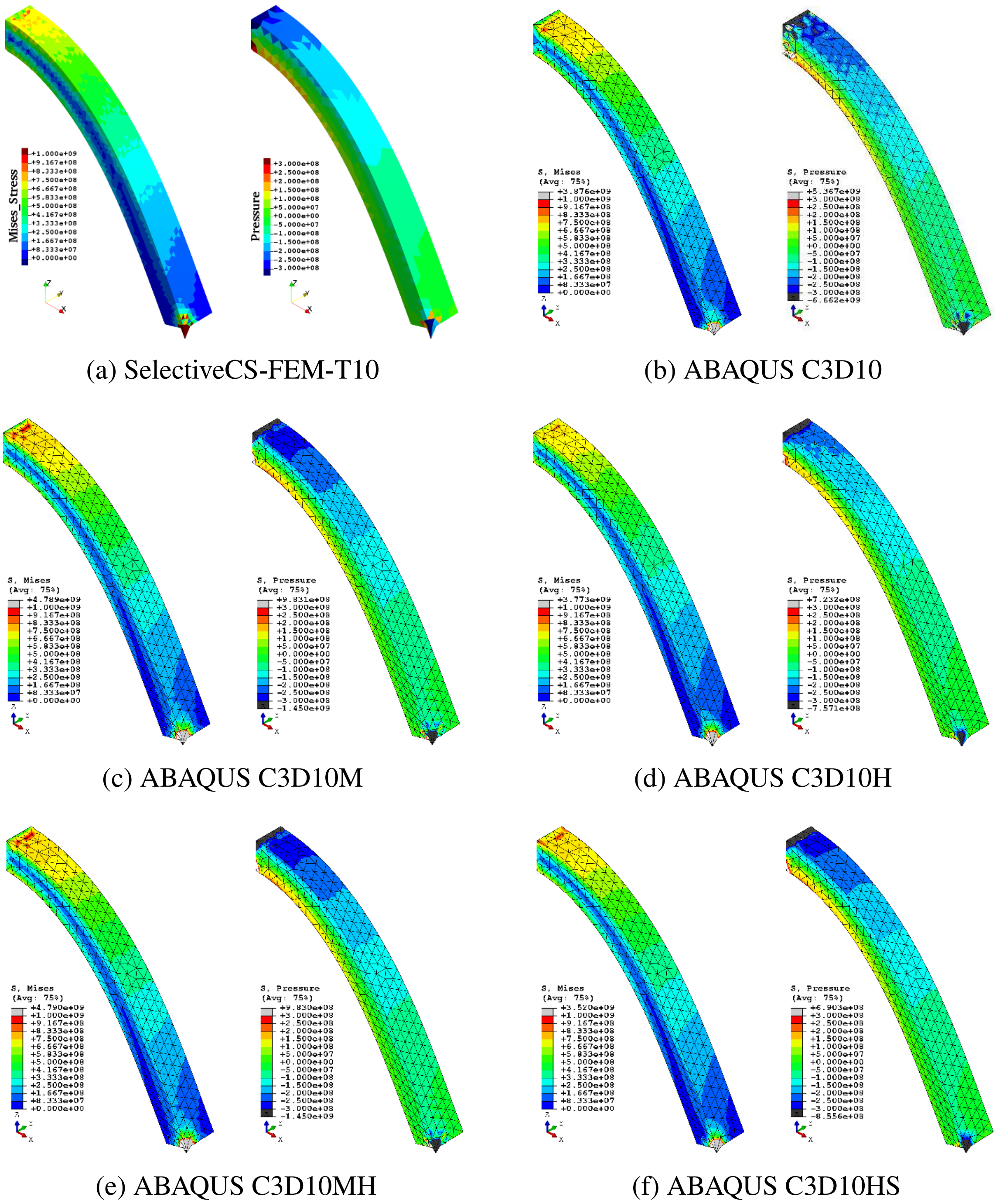

(a) SelectiveCS-FEM-T10 (b) ABAQUS C3D10

(c) ABAQUS C3D10M (d) ABAQUS C3D10H

(e) ABAQUS C3D10MH (f) ABAQUS C3D10HS

Figure 2: Comparison of Mises stress (left) and pressure (right) distributions in the cantilever bending analysis.

somewhat different each other due to stress singularity, their deformations and stress distributions have no much difference among all the methods. Looking at the deformation on the rim part carefully, we can see that the element edges are largely bent periodically at the intermediate nodes in the ABAQUS T10 elements. It is well known that the accuracy and stability of T10 elements drop greatly when the position of the intermediate node deviates largely from the mid-point of the corner nodes. In fact, all of the ABAQUS T10 elements get converge failure around 25% compression. On the other hand, SelectiveCS-FEM-T10 does not show such a bending at the intermediate nodes owing to the piecewise linear shape functions.

Fig. 4 shows the distribution of the nodal reaction forces on the top surface at the same time. Typical nodal reaction force oscillations are seen in the results of the non-modified ABAQUS elements (C3D10, C3D10H and C3D10HS), whereas SelectiveCS-FEM-T10 and the modified

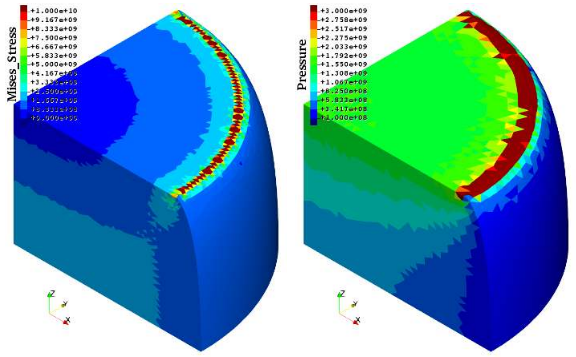

(a) SelectiveCS-FEM-T10

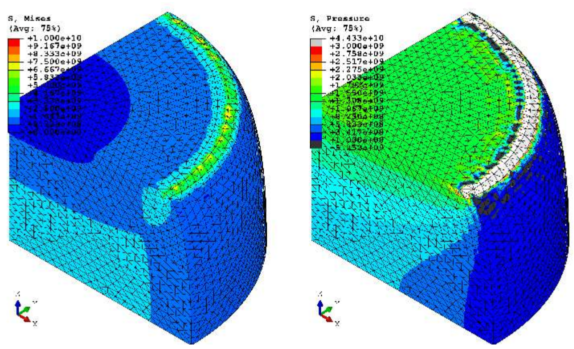

(b) ABAQUS C3D10

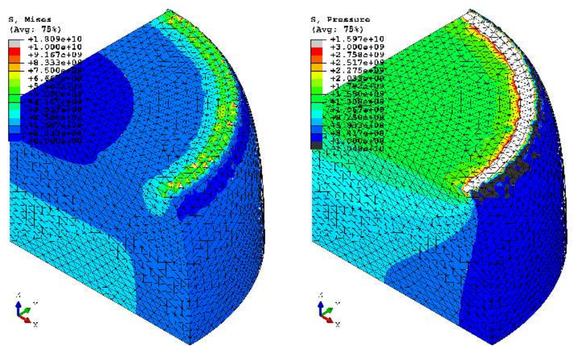

(c) ABAQUS C3D10M

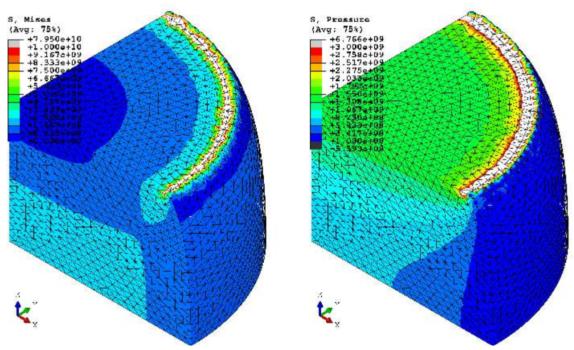

(d) ABAQUS C3D10H

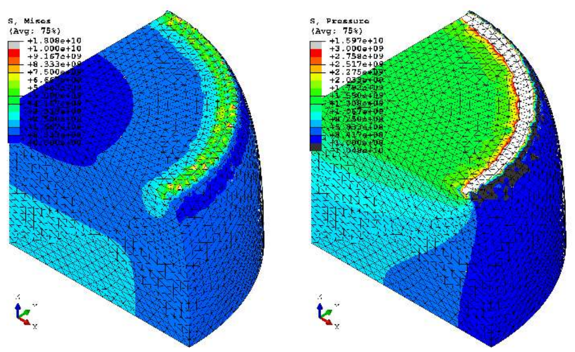

(e) ABAQUS C3D10MH

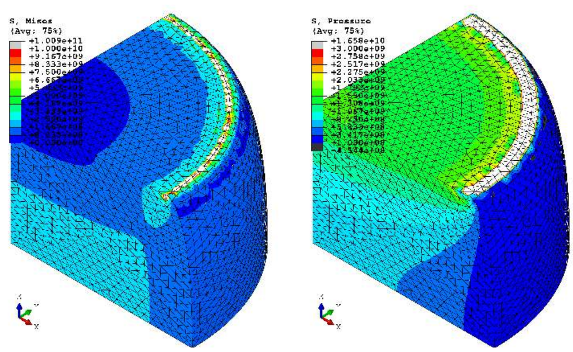

(f) ABAQUS C3D10HS

Figure 3: Comparison of Mises stress (left) and pressure (right) distributions in the cylinder barreling analysis at 24% compression states.

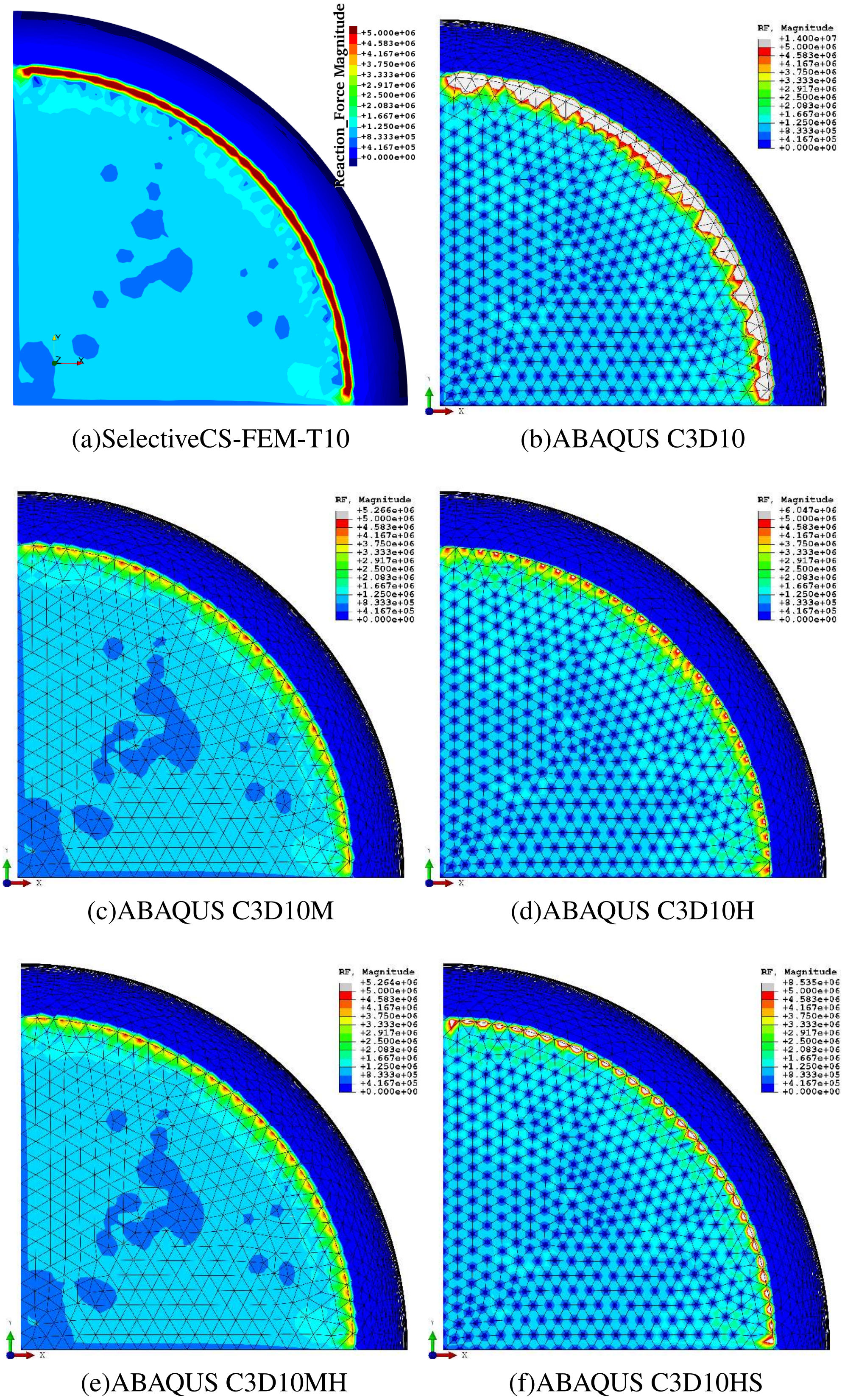

Figure 4: Comparison of nodal reaction force distributions of the upper face in the cylinder barreling analysis at 24% compression states. The proposed method (a) and the modified T10 elements of ABAQUS ((c) and (e)) represent valid distributions. In contrast, the non-modified T10 elements of ABAQUS ((b), (d) and (f)) represent oscillatory invalid distributions.

ABAQUS elements (C3D10M and C3D10MH) show valid distributions. Nodal reaction force oscillation is a severe issue especially when handling contacts, but it is confirmed that SelectiveCS-FEM-T10 avoids this issue.

As a demonstration, the distributions of Mises stress and pressure at 0.47 m enforced displacement (47% compression) are shown in Fig. 5. Only the result of SelectiveCS-FEM-T10 is shown in this figure because the ABAQUS T10 elements get convergence failure in earlier states, as mentioned above. SelectiveCS-FEM-T10 gets convergence failure at 48% compression in this case; however, it gives reasonable deformation and stress distribution until it reaches the convergence failure.

Conclusion

A novel smoothed finite element method (S-FEM) using 10-node tetrahedral (T10) element, SelectiveCS-FEM-T10, was proposed. By combining the selective reduced integration (SRI) and S-FEM with cyclic smoothing, the proposed method overcome various issues: shear/volumetric locking, pressure checkerboarding, and nodal reaction force oscillation. Unlike the conventional 4-node tetrahedral (T4) S-FEMs, the strain smoothings of the proposed method are only performed within each T10 element using T4 subelements. As a result, the proposed method can be implemented as a user-defined element of general-purpose FEM codes and also its computational time is almost equivalent to the conventional T10 elements. Moreover, like the conventional S-FEMs, the proposed method is applicable to the dynamic explicit analysis because it is a pure displacement-based finite element method.

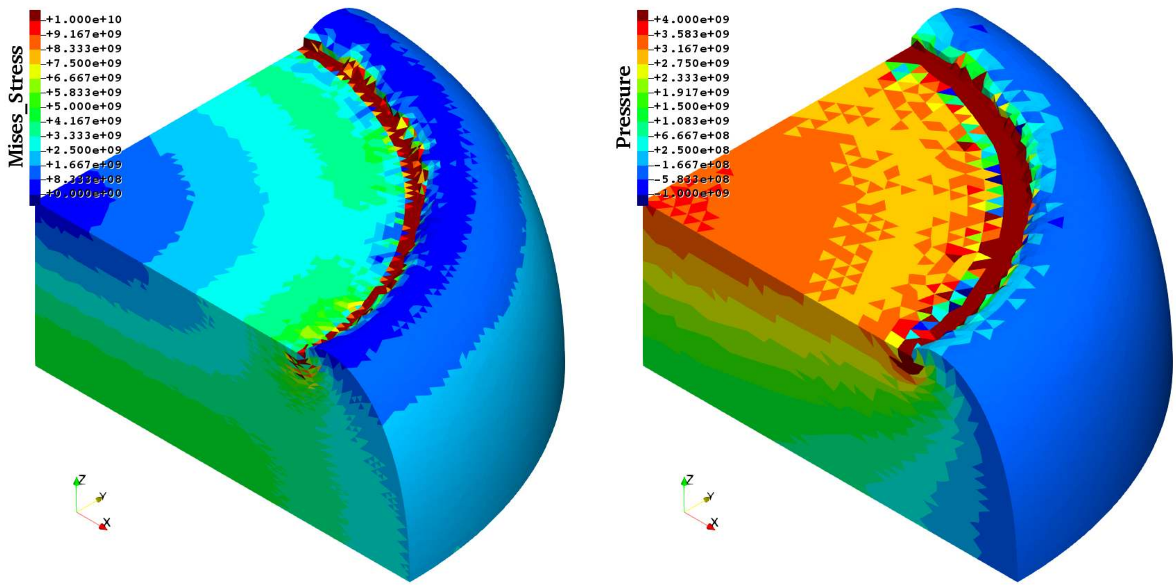

SelectiveCS-FEM-T10

Figure 5: Mises stress (left) and pressure (right) distributions of SelectiveCS-FEM-T10 in the cylinder barreling analysis at 47% compression states. Every ABAQUS T10 elements get convergence failure around 25% compression and thus their results are not shown here.

References

[1] D. S. S. Corp., *ABAQUS 6.13 Theory Guide*. Providence, RI, USA: Dassault Systèmes Simulia Corp., 2013.

[2] MSC Software Corp., *MARC 2013.1 Volume A: Theory and User Information*. Santa Ana, CA, USA: MSC Software Corp., 2013.

[3] G. R. Liu and T. Nguyen-Thoi, *Smoothed Finite Element Methods*. Boca Raton, FL, USA: CRC Press, 2010.

[4] W. Zeng and G. R. Liu, "Smoothed finite element methods (S-FEM): An overview and recent developments," *Archives of Computational Methods in Engineering*, pp. 1–39, 2016.

[5] Y. Onishi and K. Amaya, "A locking-free selective smoothed finite element method using tetrahedral and triangular elements with adaptive mesh rezoning for large deformation problems," *International Journal for Numerical Methods in Engineering*, vol. 99, no. 5, pp. 354–371, 2014.

[6] Y. Onishi and K. Amaya, "Performance evaluation of the selective smoothed finite element methods using tetrahedral elements with deviatoric/hydrostatic split in large deformation analysis," *Theoretical and Applied Mechanics Japan*, vol. 63, pp. 55–65, 2015.

[7] Y. Onishi, R. Iida, and K. Amaya, "F-bar aided edge-based smoothed finite element method using tetrahedral elements for finite deformation analysisof nearly incompressible solids," *International Journal for Numerical Methods in Engineering*, vol. 109, no. 11, pp. 1582–1606, 2017.

[8] Y. Onishi, "F-bar aided edge-based smoothed finite element method with 4-node tetrahedral elements for static large deformation elastoplastic problems," *International Journal of Computational Methods*, vol. 15, no. 1, 2018.

[9] Y. Onishi, R. Iida, and K. Amaya, "Accurate viscoelastic large deformation analysis using F-bar aided edge-based smoothed finite element method for 4-node tetrahedral meshes (F-BarES-FEM-T4)," *International Journal of Computational Methods*, vol. 17, no. 7, p. 1845003, 2018.

[10] R. Iida, Y. Onishi, and K. Amaya, "A stabilization method of F-barES-FEM-T4 for dynamic explicit analysis of nearly incompressible materials," *International Journal of Computational Methods*, in Print.

[11] E. de Souza Neto, D. Peric, M. Dutko, and D. Owen, "Design of simple low order finite elements for large strain analysis of nearly incompressible solids," *International Journal of Solids and Structures*, vol. 33, no. 20-22, pp. 3277–3296, 1996.

[12] J. T. Ostien, J. W. Foulk, A. Mota, and M. G. Veilleux, "A 10-node composite tetrahedral finite element for solid mechanics," *International Journal for Numerical Methods in Engineering*, vol. 107, no. 13, pp. 1145–1170, 2016.

[13] E. A. de Souza Neto, F. M. A. Pires, and D. R. J. Owen, "F-bar-based linear triangles and tetrahedra for finite strain analysis of nearly incompressible solids. Part I: formulation and benchmarking," *International Journal for Numerical Methods in Engineering*, vol. 62, no. 3, pp. 353–383, 2005.

[14] E. A. de Souza Neto, D. Peric, and D. R. J. Owen, *Computational Methods for Plasticity: Theory and Applications*. Hoboken, NJ, USA: Wiley, 2008.